PHYSICS OF HIGH BOOTSTRAP FRACTION, HIGH PERFORMANCE PLASMAS ON THE DIII-D TOKAMAK

M.R. Wade,[1] T.C. Luce,[2] J.R. Ferron,[2] P.A. Politzer,[2] D.P. Brennen,[3] T.A. Casper,[4] A.M. Garofalo,[5] C.M. Greenfield,[2] A.W. Hyatt,[2] R. Jayakumar,[4] J.E. Kinsey,[6] R.J. La Haye,[2] L.L. Lao,[2] E.A. Lazarus,[1] J. Lohr,[2] M.A. Makowski,[4] M. Murakami,[1] M. Okabayashi,[7] C.C. Petty,[2] R. Prater,[2] E.J. Strait,[2] A.D. Turnbull,[2] J.G. Watkins,[8] and W.P. West[2]

[1]Oak Ridge National Laboratory, Oak Ridge, Tennessee 37831, USA
[2]General Atomics, P.O. Box 85608, San Diego, California 92186-5608, USA
[3]ORISE, Oak Ridge, Tennessee, USA
[4]Lawrence Livermore National Laboratory, Livermore, California 94550, USA
[5]Columbia University, New York, New York 10027, USA
[6]Lehigh University, Bethlehem, Pennsylvania, USA
[7]Princeton Plasma Physics Laboratory, Princeton, New Jersey, USA
[8]Sandia National Laboratories, Albuquerque, New Mexico 87185-5800

Introduction. At present, conventional tokamak scenarios [1] offer the most reliable means to achieve sustained ignition in a next-generation magnetic fusion device. The plasma current I_p in these scenarios is generated almost entirely via induction from a central solenoid. Therefore, such scenarios are limited in pulse length by the engineering constraints on the solenoid. Advanced tokamak research on DIII-D is aimed at demonstrating plasma conditions in which the current profile can be generated solely via the self-generated "bootstrap current" ($I_{BS} = f_{BS}\, I_p$) and other non-inductive sources. A further goal is to accomplish this while maintaining the fusion power density ($\propto \beta \propto \beta_N/q$) and fusion gain ($\propto \beta\tau \propto \beta_N H_{89}/q^{1+\alpha}$) at levels comparable to those obtained in conventional tokamak scenarios. The achievement of a self-consistent solution that combines high bootstrap fraction $f_{BS} \propto q\beta_N \propto \beta_p$, high β, and $\beta\tau$ requires achieving high β_N and confinement factor H_{89} while operating at moderately high safety factor q. Here, $\beta_N = \beta/I_N$ where $I_N = I_p/aB_T$ is the normalized current, a is the plasma minor radius and B_T is the toroidal field, H_{89} is the energy confinement relative to the ITER89P confinement scaling ($H_{89} = \tau_E/\tau_{E,ITER89P}$) [2]. The exponent α is 1.4 in the ITER89P scaling but nondimensional scaling studies have shown $\alpha = 2$ [3]. Further constraints arise from the need to drive current non-inductively to supplement the bootstrap current. On DIII-D, the primary means of doing this are via neutral beam current drive (NBCD) and electron cyclotron current drive (ECCD). Both techniques favor operation at high plasma electron temperature (or equivalently, low density at constant β) since $I_{CD} \propto T_e P_{CD}/n_e R$. Hence, density control is essential.

Overview. Studies on DIII-D have demonstrated that plasmas with $\beta_N \sim 4.1$, $H_{89} \sim 3.0$, and $q_{min} > 1.5$ can be sustained for several energy confinement times $\tau_{dur} \sim 5\,\tau_E$ (Fig. 1). Absolute plasma parameters, simultaneously achieved, are: $\beta = 4.2\%$, $\beta\tau = 0.66\%$-s, $\beta_p \approx 2$, bootstrap current fraction $f_{BS} = 65\%$, and non-inductive current fraction $f_{NI} = 85\%$. This discharge had $I_p = 1.2$ MA and $B_T = 1.85$ T with the ion ∇B drift toward the lower divertor and was arrived at by empirical optimization of the heating profile, current ramp rate, and L-H transition timing. During the high β phase, the neutral beam power is controlled via feedback to a programmed evolution of plasma stored energy [Fig. 1(f)]. Typically in these discharges, slowly growing (~10 ms) n=1, low frequency (~100 Hz) perturbations are observed by a set of saddle loops located outside the vacuum vessel, as β increases past the empirical ideal no-wall limit ($\beta \sim 4\,\ell_i\, I_N$). The growth rate and frequency as well as the fact that these modes occur only as β exceeds the no-wall limit are consistent with the expectations for resistive wall modes (RWMs). These instabilities have been identified as the limiting factor for β in this class of discharges without active intervention [4]. However, in this case, RWM feedback stabilization is utilized via feedback control of a set of segmented coils located on the midplane of DIII-D to minimize the n=1 perturbation measured by Mirnov coils located inside the vacuum vessel [5]. Using this feedback scheme, the amplitude of the RWM is maintained below 5 G up to 1.9 s, allowing β_N to increase up to approximately $6\,\ell_i$ [Fig. 1(c)]. The large variations in β during this phase [Fig. 1(d)] are

correlated with the occurrence of giant type I ELMs. These ELMs have two effects. First, the ELMs expel a large amount of energy causing a rapid reduction in β. Second, the large magnetic fluctuations associated with the ELMs induce a transient response by the RWM feedback control algorithm that momentarily allows RWM growth. Once the ELM event is over, proper feedback control is restored and the existing RWM is quickly damped. One could argue in this case that the ELMs limit β, but since the neutral beams are feedback controlled and therefore limiting the attainable β, it is difficult to assess the impact of ELMs on β. Experiments are planned to address this issue.

The termination of high performance conditions is attributed to the onset of a n=2/m=1 neoclassical tearing mode [Fig. 1(c)] when q_{min} approaches 1.5 [Fig. 1(e)]. Theoretical analysis suggests the onset of this mode is consistent with Δ' increasing as q_{min} approaches 1.5 [6]. The current density profile early in the high performance phase at 1.3 s is peaked near the half radius, which is considered near optimal from a stability, transport, and bootstrap current standpoint. However, as the high performance phase continues, the peak in the current density profile moves inward. This occurs while the total pressure and pressure profile remain nearly constant. At 1.4 s, the Ohmic current (deduced as described in Ref. [7]) is peaked off-axis at ρ = 0.4. Within the uncertainties, the bootstrap current [8], is found to supply all of the current density near the plasma edge. In the mid-radius region, the plasma profiles produce a flat bootstrap current profile providing approximately 50% of the total current density. Model calculations of the bootstrap current drive and the NBCD using ONETWO [8] indicate only 50% of the central current density is supplied by these sources. This is due to the gentle gradients in this region (reduced bootstrap current) and the high plasma density (reduced central NBCD). Analysis of the internal loop voltage evolution indicates that the bootstrap current continually increases throughout the high performance phase. At 1.8 s, approximately 80% of the total current is supplied non-inductively, with 65% originating from the bootstrap current and 15% from NBCD.

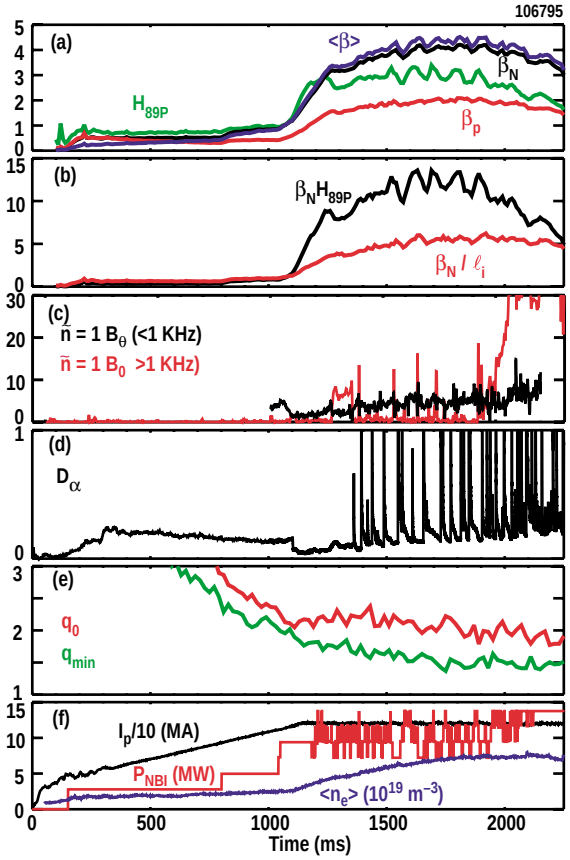

Fig. 1. Plasma parameters versus time for a discharge (106795) with $\beta_N H_{89}$ ~ 12.5 for 5 τ_E (a) From top to bottom: <β>, β_N, H_{89}, and β_p, (b) From top to bottom: $\beta_N H_{89}$ (upper trace), β_N/ℓ_i (lower trace); (c) n=1 Mirnov amplitude; (d) divertor D_α (a.u.); (e) q_0 (upper trace), q_{min} (lower trace); (f) 10x plasma current (MA), neutral beam injected power (MW), line-averaged density (10^{19} m^{-3}).

The evolution of the current density profile is believed to be the limiting factor in extending the duration of this high-performance phase. This is due to the gradual peaking of the Ohmic current owing to the highly peaked conductivity profile. To mitigate this process, we plan to replace the Ohmic current at ρ = 0.4 by off-axis ECCD. A major concern is the strong rise in the density throughout the high performance phase [Fig. 1(f)]. The magnitude of ECCD is affected strongly by this rise in density and therefore density control is essential.

Density Control. New divertor hardware was installed in early 2000 that allows divertor exhaust of high triangularity, upper single-null plasmas. Preliminary experiments using this new divertor structure have shown the divertor performance to exceed the performance of both the lower divertor in DIII-D and the previous configuration of the upper divertor [10].

A clear example of density control (both main particle and impurities) in a high performance discharge is shown in Fig. 2. This discharge has normalized performance

$\beta_N H_{89} \sim 7.5$ sustained for 4.7 s or about 26 τ_E [Fig. 2(b)]. Similar discharges have been sustained with $\beta_N H_{89} \sim 7.5$ for 6.3 s (or 35 τ_E). Due to the excellent particle control characteristics of the upper pump, feedback control of the density at $n_e = 3.6 \times 10^{19}$ m^{-3} required a small level of gas injection throughout the high performance phase [Fig. 2(c)]. In this case, the wall inventory reaches a quasi-steady-state level early in the H-mode phase and is maintained constant for the duration of the discharge, indicating a near perfect balance between particle input and particle exhaust [Fig. 2(d)]. Core impurity contamination during the high performance phase is also well regulated with the core carbon (the main impurity in DIII-D) fraction being ~ 2.5%, leading to core $Z_{eff} \sim 1.75$ [Fig. 2(e)].

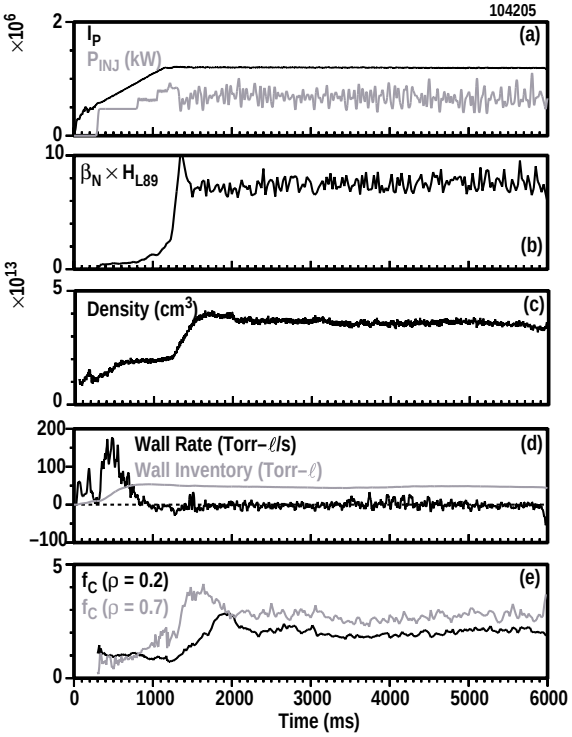

Fig. 2. Long-pulse demonstration of density and β control in a high performance discharge (a) plasma current ×10 (MA) (upper trace), actual neutral beam power (MW) (light trace), and averaged (50 ms) neutral beam power (MW) (lower trace); (b) $\beta_N H_{89}$; (c) line-averaged density (10^{19} m^{-3}) and D_2 gas puffing; (d) wall inventory (solid line) and wall fueling/degassing rate (dashed line), and (e) impurity concentration at normalized radii $\rho = 0.2$ (solid line) and $\rho = 0.7$ (dashed line).

Experiments using this new divertor have been successful in maintaining density levels in high performance plasmas commensurate with the ECCD requirements. However, it has proven difficult to reproduce the high normalized performance of the discharge shown in Fig. 1. By necessity, the pumped discharges are required to be magnetically unbalanced towards the upper divertor (denoted by the distance at midplane between the flux tubes connecting to each X-point, dRsep) such that adequate particle flux is directed at the upper divertor for exhaust. Typically, dRsep > 5 mm is required, which results in a decrease in the edge safety factor q_{95} and the plasma shape parameter [11] $S = I_N q_{95}$. Data from 1999–2000 suggested that this reduction in the achievable β_N was consistent with a reduction in the shape parameter S [see open triangles in Fig. 3(a)]. This hypothesis was consistent with previous theoretical calculations that showed that the n=1 ideal stability limit increased as S increased [12]. However, because the experiments in 1999–2000 were done at a fixed value of I_N, it was not possible to separate this dependence on S from a possible dependence on q_{95}. Studies in 2001 sought to decouple this correlated dependence by varying the toroidal field from 1.6 T to 2.1 T on successive discharges with the plasma shape held constant. A comparison of this recent data with the 1999–2000 data set is shown in Fig. 3. This data suggests that the β limit most strongly depends on q_{95} while little dependence on S is now apparent. Theoretical calculations using the GATO code indicate a weak dependence of the no-wall, n=1 ideal stability limit on q_{95}.

ECCD. Because density control is crucial for adequate ECCD efficiency, ECCD studies to date have been conducted at somewhat reduced plasma parameters from the best cases. This is an example of the compromise that must be made in integrating the physics of seemingly unrelated constraints (e.g., density control, high β_N). The ECCD target discharge had a similar temporal evolution as the discharge in Fig. 1 with $I_p = 1.1$ MA, $B_T = 1.75$ T, and dRSep = 5 mm. Neutral beam feedback control was used to maintain $\beta_N \sim 3.3$. Approximately 2 MW of ECCD, configured for co-current drive on the inboard midplane at $\rho = 0.3$, was applied starting at 1.3 s and maintained until 2.3 s. The line-averaged density increased slightly throughout the ECCD phase, varying from $4.5–5.0 \times 10^{19}$ m^{-3}. Through simulation of the response of the MSE data to the application of ECCD, the total current driven in this case is found to be ~ 78 ± 20 kA. This is consistent with the prediction of 80 kA by the CQL-3D collisional Fokker-Planck code. A comparison of the theory and the

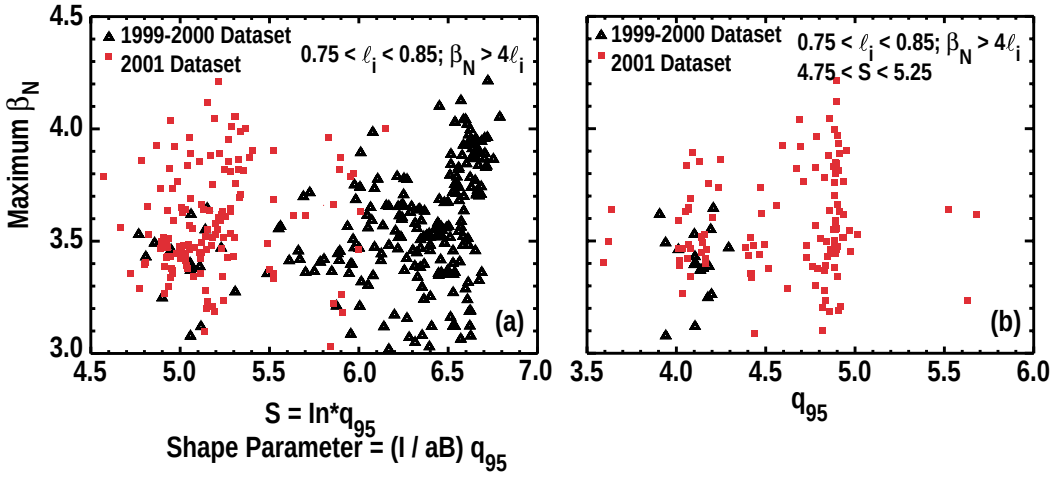

Fig. 3. Measured β_N limit versus (a) shape parameter S and (b) q_{95} at fixed shape. Triangless are from 1999–2000 data set. Squares are from 2001. Data set is restricted to cases with $\beta_N > 4\,\ell_i$ and $0.75 < \ell_i < 0.85$.

experiment for L-mode, H-mode, and this high performance case is shown in Fig. 4. The consistency between the CQL-3D predictions and the experimental measurements in these cases provides confidence that the CQL-3D model can be used as a predictive tool in determining the optimum conditions for off-axis ECCD. The prediction for the ECCD efficiency required for sustaining the current density profile in the high bootstrap fraction target scenario is shown on the right hand side of Fig. 4.

Summary. In summary, the major elements in achieving integrated advanced tokamak performance (namely, high β, density control, ECCD) have been demonstrated on DIII-D. High performance plasmas that simultaneously combine high normalized performance with $\beta_N \sim 4$, $H_{89} \sim 3.0$, and $f_{BS} \sim 60\%$, with $q_{min} > 1.5$ have been sustained for several energy confinement times. The β limit in these plasmas is significantly above the no-wall, n=1 ideal stability limit with $\beta_N \sim 6\,\ell_i$ as a result of active feedback stabilization of RWMs. Furthermore, density control compatible with high ECCD efficiency as well as ECCD efficiency consistent with maintaining the current density profile with projected EC power levels have been demonstrated. The integration of these elements still remains a challenge as present experiments are unable to sustain high β simultaneous with density control.

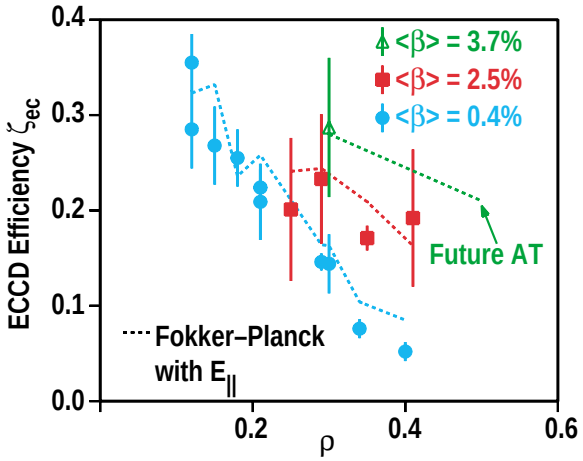

Fig. 4. Comparison of measured ECCD efficiency (symbols) versus Fokker-Planck prediction (dashed lines) for L-mode (circles), H-mode (squares), and high bootstrap fraction, advanced tokamak discharges (open triangles).

Work supported by U.S. Department of Energy under Contracts DE-AC03-99ER54463, DE-AC05-00OR22725, W-7405-ENG-48, DE-AC04-94AL85000, DE-AC02-76CH03073, and Grants DE-AC05-76OR00033, DE-FG02-89ER53297, DE-FG02-92ER54141.

[1] ITER Physics Basis, Nucl. Fusion **39**, (1999) 2137.
[2] ITER Physics Basis, Nucl. Fusion **39**, (1999) 2175.
[3] C.C. Petty, et al., Phys. Plasmas **5**, (1998) 1695.
[4] M.R. Wade et al., Phys. Plasmas **8** (2001) 2208.
[5] M. Okabayashi, et al., Phys. Plasmas **8** (2001) 2071.
[6] D. Brennan, et al., this conference.
[7] C.B. Forest, et al., Phys. Rev. Lett. **73**, (1994) 2444.
[8] O. Sauter, C. Angioni, Y.R. Lin-Liu, Phys. Plasmas **6**, (1999) 7834.
[9] H.E. St John, T.S. Taylor, Y.R. Lin-Liu, A.D. Turnbull, Plasma Phys. and Contr. Nucl. Fusion Research, Seville, 1994 (IAEA, Vienna, 1995) Vol. **3**, p. 603.
[10] M.A. Mahdavi, et al., J. Nucl. Mater. **290-293** (2001) 905.
[11] E.A. Lazarus, et al., Phys. Fluids B **4**, (1992) 3644.
[12] A.D. Turnbull, et al., Nucl. Fusion **38**, (1998) 1467.